Journal of Geophysical Research: Space Physics

RESEARCH ARTICLE
10.1029/2018JA025183

Key Points:
- Simultaneous observations of KHWs in the midtail and the near-Earth space
- KHWs possibly increase their sizes toward the tail
- Potential evidence of dawn-dusk asymmetry in the KHWs

Supporting Information:
- Supporting Information S1
- Movie S1

Correspondence to:
Q. Shi,
sqq@sdu.edu.cn

Citation:
Ling, Y., Shi, Q., Shen, X.-C., Tian, A., Li, W., Tang, B., et al. (2018). Observations of Kelvin-Helmholtz waves in the Earth's magnetotail near the lunar orbit. *Journal of Geophysical Research: Space Physics*, *123*, 3836–3847. https://doi.org/10.1029/2018JA025183

Received 4 JAN 2018
Accepted 22 APR 2018
Accepted article online 30 APR 2018
Published online 23 MAY 2018

Observations of Kelvin-Helmholtz Waves in the Earth's Magnetotail Near the Lunar Orbit

Yiming Ling[1,2,3], Quanqi Shi[1], Xiao-Chen Shen[1], Anmin Tian[1], Wenya Li[2,4], Binbin Tang[2], A. W. Degeling[1], Hiroshi Hasegawa[5], Motoharu Nowada[1], Hui Zhang[6], I. J. Rae[7], Qiu-Gang Zong[8], Suiyan Fu[8], A. N. Fazakerley[7], and Zuyin Pu[8]

[1]Shandong Provincial Key Laboratory of Optical Astronomy and Solar-Terrestrial Environment, School of Space Science and Physics, Shandong University, Weihai, China, [2]State Key Laboratory of Space Weather, National Space Science Center (NSSC), Chinese Academy of Sciences, Beijing, China, [3]CAS Key Laboratory of Geospace Environment, School of Earth and Space Sciences, University of Science and Technology of China, Hefei, China, [4]Swedish Institute of Space Physics, Uppsala, Sweden, [5]Institute of Space and Astronautical Science, Japan Aerospace Exploration Agency (JAXA), Sagamihara, Japan, [6]Geophysical Institute, University of Alaska Fairbanks, Fairbanks, AK, USA, [7]Mullard Space Science Laboratory, University College London, Dorking, UK, [8]School of Earth and Space Sciences, Peking University, Beijing, China

Abstract Kelvin-Helmholtz waves (KHWs), which have been widely observed at the magnetopause in the region near the Earth, play an essential role in the transport of solar wind plasma and energy into the magnetosphere under dominantly northward interplanetary magnetic field (IMF) conditions. In this study, we present simultaneous observations of KHWs under the northward IMF observed by both the Acceleration, Reconnection, Turbulence, and Electrodynamics of Moon's Interaction with the Sun (ARTEMIS) spacecraft in the Earth's magnetotail around the lunar orbit (at $X \sim -50R_E$, $Y \sim 30R_E$, dusk side) and the Geotail in the near-Earth space (at $X \sim -5R_E$, $Y \sim -10R_E$, dawn side). The KHWs are quantitatively characterized by their dominant period, phase velocity, and wavelength, utilizing wavelet analysis and an approximation of their center-of-mass velocity. Our results suggest that the phase velocity and spatial scale of KHWs may increase as they propagate along the boundary layer toward the tail. Alternatively, the differences between the ARTEMIS and Geotail observations may indicate the possibility of dawn-dusk asymmetry in the excited KHWs in this study. Our results strongly evidence the existence of the development of KHWs in terms of their wave frequency and scale size in the magnetotail and provide insight to the time evolution of KHWs along the magnetopause.

1. Introduction

The magnetopause, as the outer boundary of the terrestrial magnetosphere, is a critical region for entry of energy and particles from the solar wind into the magnetosphere. Usually, low-latitude magnetic reconnection along the dayside magnetopause facilitates the transportation of energy and mass during southward interplanetary magnetic field (IMF) periods (Dungey, 1962). However, the situation is less clear for periods of northward IMF, as dayside magnetic reconnection is less efficient under these conditions. Several possible mechanisms for the transport of solar wind plasma, momentum, and energy across the magnetopause under northward IMF have been proposed (e.g., Gou et al., 2016; Shi et al., 2013; Song & Russell, 1992; Terasawa et al., 1997). The Kelvin-Helmholtz instability (KHI), excited by velocity shear near the magnetopause, is one of the possible mechanisms of plasma entry (e.g., Chandrasekhar, 1961; Fairfield et al., 2000; Hasegawa et al., 2004; Liu et al., 2018). Besides the energy transport into the magnetosphere, KHI along the magnetopause also excites ultra low frequency (ULF) waves in the magnetosphere (e.g., Chen & Hasegawa, 1974; Rae et al., 2005; Wang, Thorne, et al., 2017), which play an important role in many dynamic processes, such as auroral activity and transport of radiation belt electrons. Recently, Kavosi and Raeder (2015) found that the occurrence probability of Kelvin-Helmholtz waves (KHWs) is ~19% regardless of the solar wind conditions and also an important KH activity for southward IMF, when low-latitude magnetic reconnection dominates and prevents KHWs growth; hence, KHWs may be more important for the plasma entry than previously thought. Moreover, previous studies have indicated that the KHI contributes to the formation of the low-latitude boundary layer during periods of northward IMF (e.g., Mitchell et al., 1987; Taylor et al., 2008). Song and Russell (1992) predicted theoretically that high-latitude lobe reconnection would form the low-latitude boundary layer. However, Taylor et al. (2008) showed simultaneous

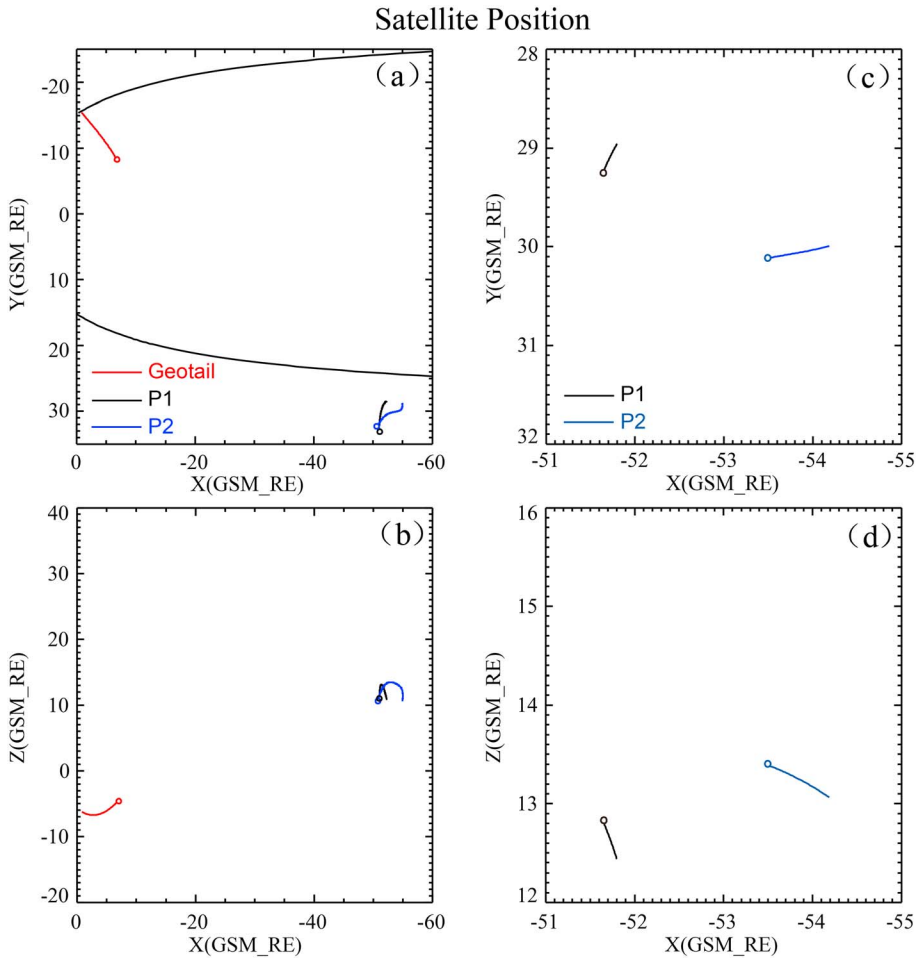

Figure 1. Orbit of ARTEMIS (P1, in black; P2, in blue) and Geotail (red) spacecraft in the GSM coordinates: (a, b) The satellite position from 19:00 UT, 13 March, to 02:00 UT, 14 March 2014, and (c–d) the locations of ARTEMIS mission from 23:35 UT, 13 March, to 00:13 UT, 14 March 2014. The location of magnetopause, as shown in curved black line, is calculated based on the Shue et al. (1998) model with the solar wind dynamic pressure P_{dyn} = 3.0 nPa and B_z = 2.0 nT.

observational evidence of high-latitude reconnection by the IMAGE spacecraft and ground-based instruments, as well as KHWs by the TC-1 spacecraft at the magnetopause, supporting the notion that not only high-latitude reconnection but also KHI makes nonnegligible contribution to the formation of the low-latitude boundary layer.

The KHWs have been studied extensively using both in situ observations and simulations. With observations by the four Cluster spacecraft, Hasegawa et al. (2004) found that KHWs can grow nonlinearly, and the resultant rolled-up vortices can mix the solar wind and magnetospheric plasmas. Takagi et al. (2006) showed that the detection of low-density and faster-than-sheath magnetospheric plasma can be taken as a marker of rolled-up vortices. This typical feature, together with quasi-periodic fluctuations (periods of 1–5 min) in the plasma parameters and magnetic fields under northward IMF, can be used as criteria to identify rolled-up vortices in single-spacecraft observations (Hasegawa et al., 2006; Taylor et al., 2012). The wavelength, phase velocity, and period were used to quantitatively characterize the KHWs by Foullon et al. (2008). Additionally, a statistical survey has been carried out to investigate the influence of solar wind conditions on the development of KHWs (Lin et al., 2014). The KHW period is found to be shorter for higher solar wind velocity and smaller IMF clock angle. Recently, the high-resolution plasma data obtained by the Magnetospheric Multiscale mission provides the first opportunity to directly investigate the evidence of reconnection due to KHWs, which leads to direct plasma transfer across the shear layer inside KH vortices (e.g., Eriksson, Lavraud, et al., 2016; Eriksson, Wilder, et al., 2016; Li et al., 2016).

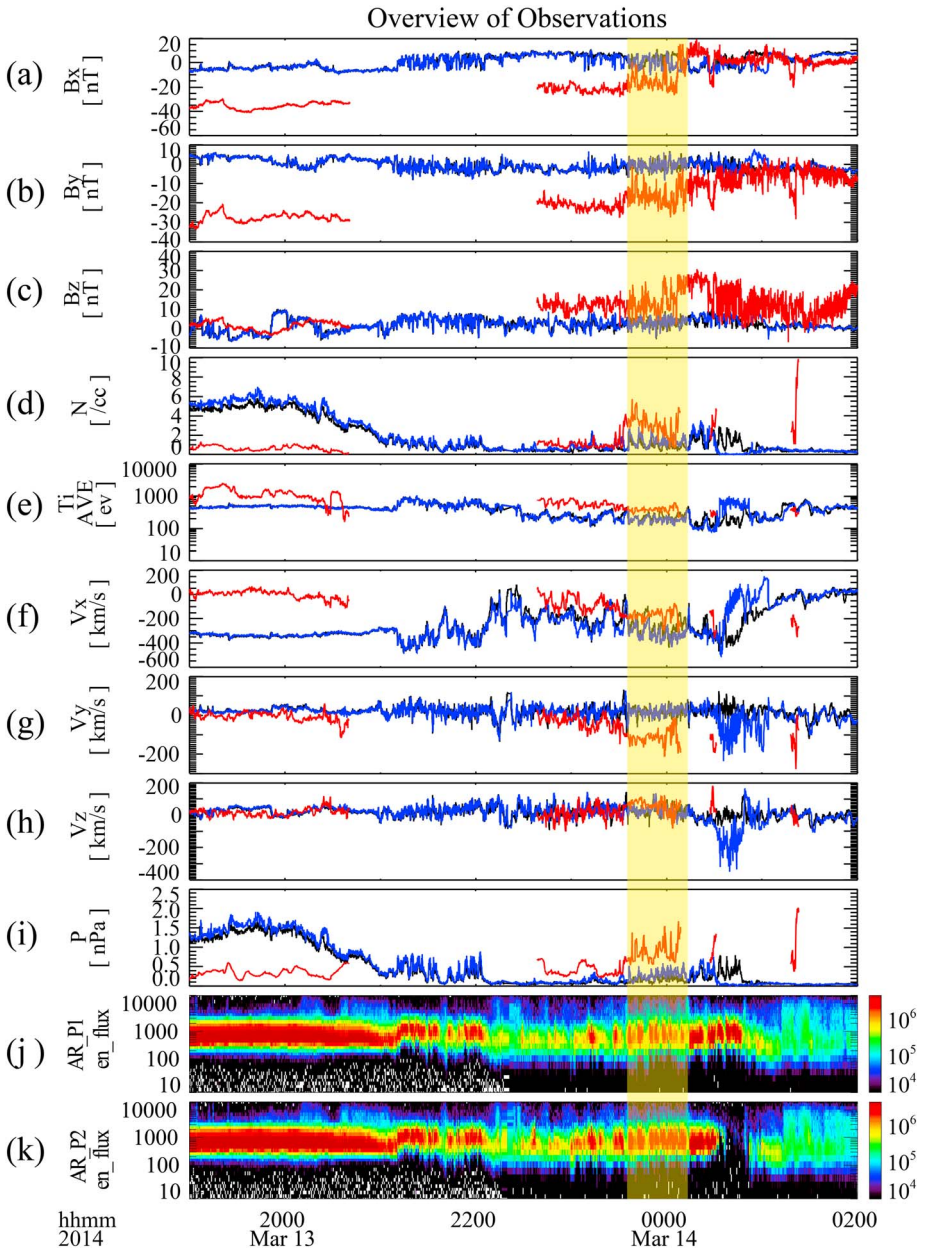

Figure 2. Time series data in GSM coordinates taken by Geotail (in red), ARTEMIS-P1 (in black) and P2 (in blue) from 19:00 UT, 13 March, to 02:00 UT, 14 March 2014: (a–c) Three components of the magnetic field, (d) ion number density, (e) average ion temperature, (f–h) three components of the bulk velocity, (i) total pressure, and (j–k) energy flux of ions at P1 and P2, respectively. The yellow shaded region indicates the interval of interest.

The time evolution of KHWs has long been discussed. Some computational studies have shown that in the nonlinear stage of the KHW evolution, small-scale vortices will be born within the larger scale parent KH vortices; thus, KH vortices are found to decay and break into turbulence (Matsumoto & Hoshino, 2004; Nakamura et al., 2004). However, other numerical simulations suggest that small vortices can merge along the magnetopause and evolve into large-scale vortices in the magnetotail (Miura, 1999). This so-called "inverse cascade" is a candidate mechanism to explain how wavelengths longer than predicted by linear theory can be observed (Belmont & Chanteur, 1989). Since the previous observations are mainly reported in the near-Earth region, the issue of how KHWs develop further downtail remains a subject of debate. Lately, Wang, Merkin, et al. (2017) reported events with transient perturbations in plasma and magnetic field parameters (B_x) by Acceleration, Reconnection, Turbulence and Electrodynamics of Moon's Interaction with the Sun

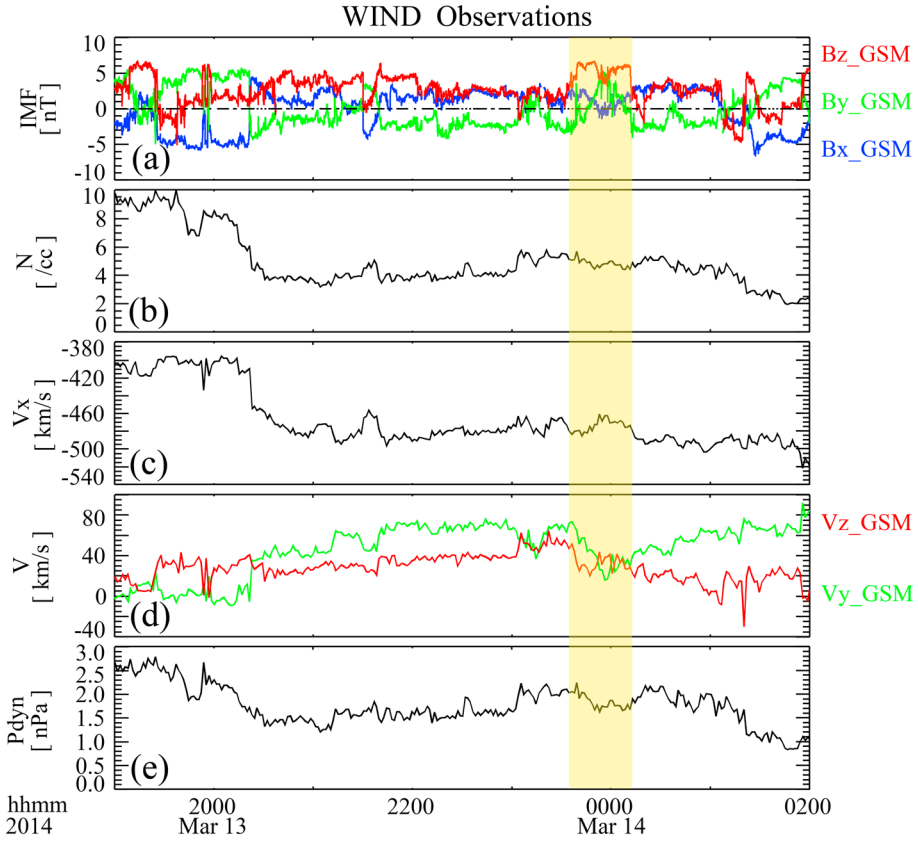

Figure 3. Solar wind conditions seen by the WIND spacecraft (time shifted 60 min forward): (a) Three components of the IMF, (b) ion number density, (c–d) three components of the bulk velocity, and (e) dynamic pressure. The yellow shaded region indicates the interval of interest.

(ARTEMIS) observations under steady northward IMF conditions and attributed them to KH vortices in the midtail. It is necessary to cover both terrestrial space and the magnetotail with more observations in order to provide more detailed benchmarks for theoretical modeling of nonlinear KH dynamics and plasma transport processes along the magnetopause.

In this article, we study an event observed by the ARTEMIS spacecraft in the magnetotail on 13 and 14 March 2014, and we also present simultaneous observations by the Geotail spacecraft in the region near the Earth. The paper is organized as follows. In section 2, we introduce the data used. Section 3 presents the observations and analysis results. Section 4 gives a discussion and summary.

2. Data

The Time History of Events and Macroscale Interactions during Substorms (THEMIS) spacecraft was launched on 17 February 2007 (Angelopoulos, 2008). The mission contains five probes (THA, THB, THC, THD, and THE). Since 2010, THB and THC were retasked to orbit the moon and have become the ARTEMIS mission, while the three remaining probes continue to orbit Earth. In this study, we use 3-s resolution data from the ARTEMIS mission. The fluxgate magnetometer (FGM) (Auster et al., 2008) onboard each probe provides magnetic field data, and thermal (5 eV–25 keV) ion data are taken from the electrostatic analyzer (ESA) (McFadden et al., 2008), while ion velocity data are taken from onboard plasma moments (MOM). The low-energy particle experiment (LEP) onboard Geotail (Mukai et al., 1994) offers plasma moment data, and the magnetic field experiment (MGF) (Kokubun et al., 1994) provides magnetic field data. In particular, we used Geotail data measured by the LEP-EA instrument in RAM-A mode only, which is more reliable in the boundary region (Hasegawa et al., 2006). Time resolutions are approximately 12 and 3 s for the LEP and MGF data, respectively. The WIND spacecraft, which was 238R_E away from the Earth (upstream), monitored IMF and solar wind conditions.

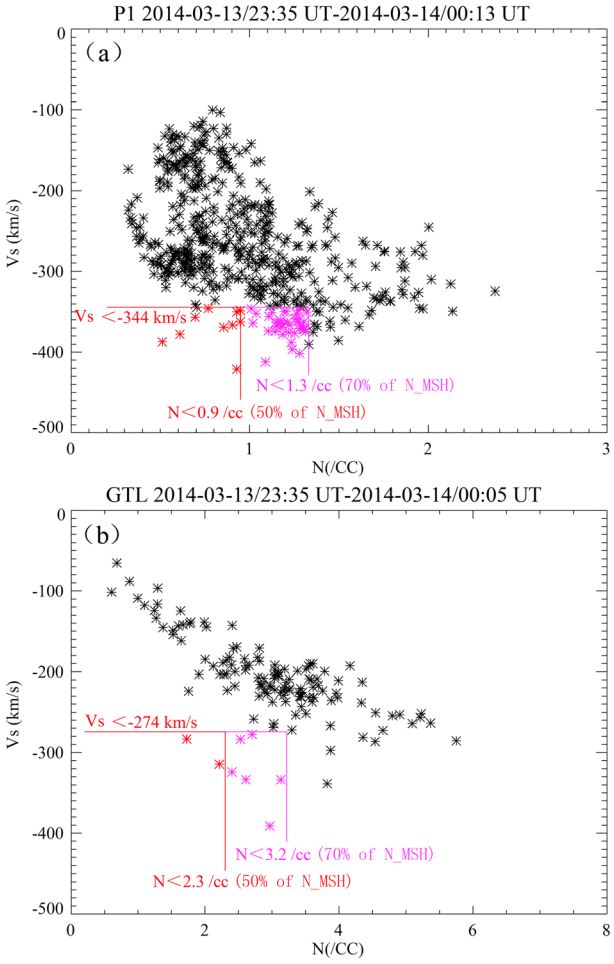

Figure 4. A scatterplot of velocity *s* component (V_s; the *s* direction is antiparallel to the averaged ion velocity for the interval of interest) versus ion number density (N): (a) P1 data for interval 23:35 UT, 13 March, to 00:13 UT, 14 March; (b) Geotail data for interval 23:35 UT on 13 March to 00:05 UT on 14 March. The red and magenta regions bounded by solid lines refer to the low-density and faster-than-sheath component of the data.

3. Observations

We have surveyed the ARTEMIS data from January 2010 to December 2014 to obtain a database of about 100 magnetopause crossings close to the lunar orbit and identified three candidate KHW events according to the criteria used by Hasegawa et al. (2006) and Taylor et al. (2012). In this study, we focus on an event on 13 and 14 March 2014, as there are simultaneous observations of three satellites (ARTEMIS P1, P2, and Geotail) in this event, which can help us understand the evolution of KHW along the magnetopause.

3.1. Overview

Figures 1a and 1b show the locations of ARTEMIS (P1 and P2) and Geotail in GSM coordinates from 19:00 UT, 13 March, to 02:00 UT, 14 March. The ARTEMIS mission was in the magnetotail near the lunar orbit (X_{GSM} = ~ $-50R_E$, Y_{GSM} = ~$30R_E$, Z_{GSM} = ~$10R_E$), and the Geotail spacecraft crossed the magnetopause in near-Earth trajectories (X_{GSM} = ~ $-5R_E$, Y_{GSM} = ~ $-10R_E$, Z_{GSM} = ~ $-5R_E$). Figures 1c and 1d show the position of the ARTEMIS spacecraft during the interval 23:35 UT, 13 March, to 00:13 UT, 14 March, which is the interval of interest for subsequent analyses. An overview of observations by the ARTEMIS (P1 and P2) and Geotail spacecraft on 13 and 14 March 2014 is shown in Figure 2. From 19:00 UT to 21:10 UT on 13 March, the ARTEMIS spacecraft was located in the magnetosheath, where the density was larger than 1 cm^{-3} (Figure 2d) and the ion energy ranges from 100 eV to 1 keV (Figures 2j and 2k). From 21:10 UT on 13 March to about 00:48 UT on 14 March, P1 and P2 entered a magnetospheric boundary layer region, which is characterized by lower density (Figure 2d), higher temperature (Figure 2e), and obvious quasi-periodic fluctuations of plasma parameters and magnetic fields (Figures 2a–2c). Meanwhile, the ion energy flux spectrogram shown in Figures 2j and 2k indicates a mixture of cold-dense magnetosheath-like plasma and hot-tenuous magnetosphere-like plasma. Around 00:48 UT on 14 March, ARTEMIS-P1 moved into the magnetosphere with a rapid decrease in the number density and velocity, and the probe remained in the magnetosphere for the remainder of the interval. ARTEMIS-P2 was 2–3R_E earthward from P1 (see Figure 1) and entered the magnetosphere ~15 min earlier than P1. The total pressure, as shown in Figure 2i, was not rigidly constant around the magnetopause. In the initial stage of the KHI, there would be no significant total pressure fluctuations around the magnetopause. As the KHI grows to a nonlinear phase and generates rolled-up vortices, the centrifugal forces push out plasmas from the center of the vortices, and thus, there is a minimum in the total pressure at the central part of the vortices and a maximum at the edge (e.g., Hasegawa, 2012). The total pressure variations mean that some of the vortices encountered were rolled up, and its observed level is consistent with observations of the KHWs (e.g., Hasegawa, 2012; Hasegawa et al., 2009).

Figure 3 shows the corresponding solar wind conditions provided by the WIND spacecraft, which have been shifted forward by 60 min considering the solar wind transit time from the position of WIND ([238, 72, 47]R_E in GSM coordinates) to ARTEMIS. The data show relatively quiet solar wind flow under generally northward IMF conditions during the boundary layer interval of interest (the yellow shaded region). The averaged IMF is [1.20, 0.88, 5.33] nT during this time interval.

3.2. Data Analysis

Here we make a close inspection of the interval of interest when the ARTEMIS and Geotail spacecraft detected clear KHW signals. As mentioned previously, the low-density and high-velocity feature seen in the data suggests the existence of rolled-up vortices (Hasegawa et al., 2006). Following the method of Hasegawa et al.

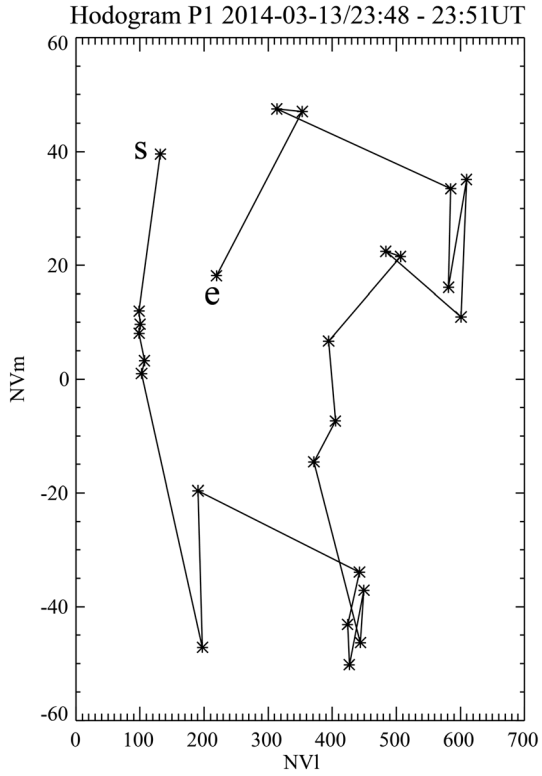

Figure 5. A hodogram of NVl versus NVm shows the plasma vortex in the *LMN* coordinates. The "s" and "e" refer to the starting and ending data points during interval 23:48–23:51 UT on 14 March.

(2006), we define a vector "*s*" directed antiparallel to the averaged ion velocity for the interval of interest (for ARTEMIS-P1: s = [0.99, −0.07, −0.13] in GSM; for Geotail: s = [0.80, 0.54, −0.27] in GSM). Figure 4 presents a scatterplot of the s component of the bulk velocity, V_s, versus the ion density, N, during the interval from 23:35 UT, 13 March, to 00:13 UT, 14 March. Figures 4a and 4b are for ARTEMIS-P1 and Geotail, respectively. The magenta region is quantitatively defined using the method proposed by Taylor et al. (2012). The value N_MSH is defined as 80% of the maximum density during this period, and the upper threshold for density is set to be 70% of N_MSH. The threshold for ion velocity is obtained from the averaged velocity for all points with density higher than N_MSH. It should be noted that the plasma from the magnetospheric side of the velocity shear layer where the KH vortex is formed should have the faster-than-sheath signature. In order to provide a more stringent estimate of the magnetospheric plasma, a stricter threshold for density of 50% of N_MSH is also used, and the corresponding points are marked with red. Because the Geotail data have lower time resolution (12 s) and measured by the LEP-EA instrument in RAM-A mode only, the number of data points satisfying the criteria is only a few in Figure 4b but is acceptable. The detection of plasma with low density and high speed suggests that a vortex or "rolled up" structure is generated near the boundary.

Minimum variance analysis (MVA) on mass flux (MVA_NV) is used to further confirm the possibility of a vortex structure (Sonnerup & Scheible, 1998). Figure 5 presents a hodogram of the plasma flow from 23:48 to 23:51 UT on 14 March (3 min) for ARTEMIS-P1. The anticlockwise rotation of the vector in the NVl and NVm plane suggests that a vortex exists in the boundary. The GSM coordinates of L, M, and N are (−0.99, 0.01, 0.15), (0.11, −0.65, 0.75), and (0.11, 0.76, 0.64), so the L direction is mainly along the anti-X direction in the GSM coordinates during this interval.

The KHW properties are characterized by their frequency and phase velocity. The wavelength can be estimated by multiplying the phase velocity and wave period. Figure 6 shows the ARTEMIS-P1 data and wavelet spectrum analysis of plasma parameters and the magnetic field for the interval 23:35 UT, 13 March, to 00:13 UT, 14 March. The fluctuations have noticeable power at a frequency of ~2 mHz (500 s) during the whole wave interval, and another peak in wave power is observed at a frequency of ~4 mHz (250 s) from 23:50 UT on 13 March to 00:05 UT on 14 March.

Figure 7 is in the same format as Figure 6, showing the magnetic field measured by Geotail and their wavelet spectra for the interval 23:35 UT, 13 March, to 00:05 UT, 14 March. The LEP-EA instrument on Geotail changed mode (RAM-A or RAM-B) multiple times during the interval of interest, so the wavelet analysis was performed only for the magnetic field data. Geotail observed waves with peaks in spectral power at two frequencies of ~3 (333 s) and ~6 mHz (167 s), as shown in Figure 7. The KHWs with two frequency ranges have been reported in previous observations (Hasegawa et al., 2009). For Geotail, the 6-mHz frequency is more common and thus could be the fundamental mode (Hasegawa et al., 2006), and the 3-mHz mode may be a signature of inverse cascade. For ARTEMIS, the 2-mHz mode may be a signature of inverse-cascade or vortex pairing. This phenomenon is further discussed in section 4.

According to the linear MHD theory for KHWs on a zero-thickness surface, the phase velocity is equal to the center-of-mass velocity ("1" and "2" refer to the magnetosphere and magnetosheath, respectively; Chandrasekhar, 1961). However, in a layer with finite thickness, the phase velocity is in between the average velocity and center-of-mass velocity (Hasegawa et al., 2009). Considering the situation where the velocity of the background magnetosphere and magnetosheath are basically unavailable, we chose the center-of-mass velocity to estimate the phase velocity in this event. This approximation is not accurate when spacecraft trajectories deviate from the center of the vortex. The period, phase velocity, and spatial scale calculated from

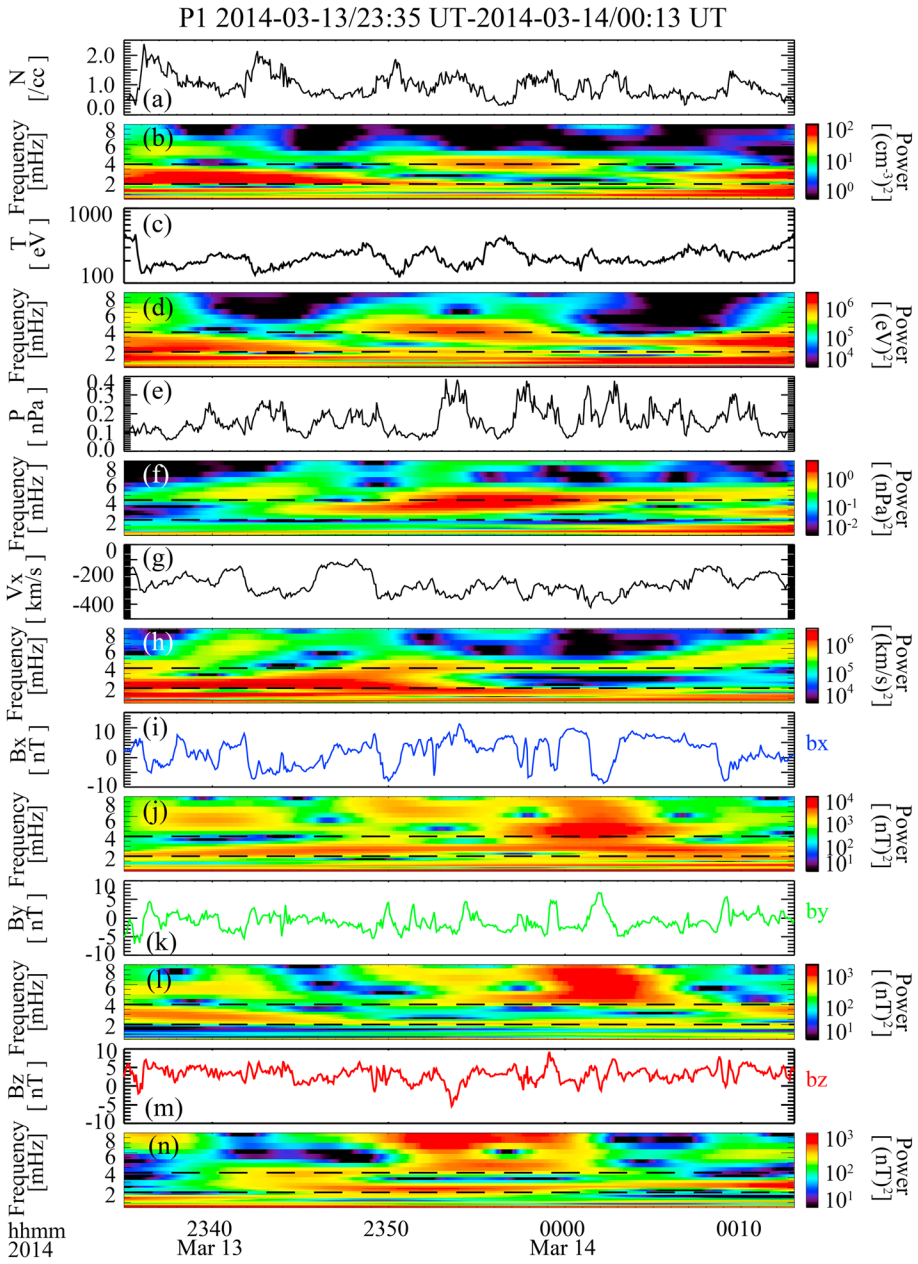

Figure 6. ARTEMIS-P1 observations for interval 23:35 UT, 13 March, to 00:13 UT, 14 March: (a) ion number density, (b) wavelet power spectrum of *N*, (c) average ion temperature, (d) wavelet power spectrum of *T*, (e) total pressure, (f) wavelet power spectrum of *P*, (g) *x* component of the bulk velocity, (h) wavelet power spectrum of V_x, (i, k, m) three components of the magnetic field, and (j, l, n) wavelet power spectrum of B_x, B_y, and B_z, respectively. The black dashed lines mark the frequencies of 2 and 4 mHz, respectively.

ARTEMIS and Geotail data are listed in Table 1. Comparing the results gained via data from the two satellites at different locations, both the phase velocity and the spatial scale of the KHWs tend to increase with distance from the subsolar point along the magnetopause.

Figure 8 shows the magnetic field and plasma parameters observed by ARTEMIS-P1 during the interval of interest, with points that correspond to the magenta and red region in Figure 4a. Many of the red points are in higher-temperature regions, which suggests that they are from the magnetospheric side, suggesting the presence of rolled-up vortices. These points are mostly concentrated from 23:50 UT, 13 March, to 00:05 UT, 14 March, suggesting that the low-density and high-velocity flows correspond to waves with higher

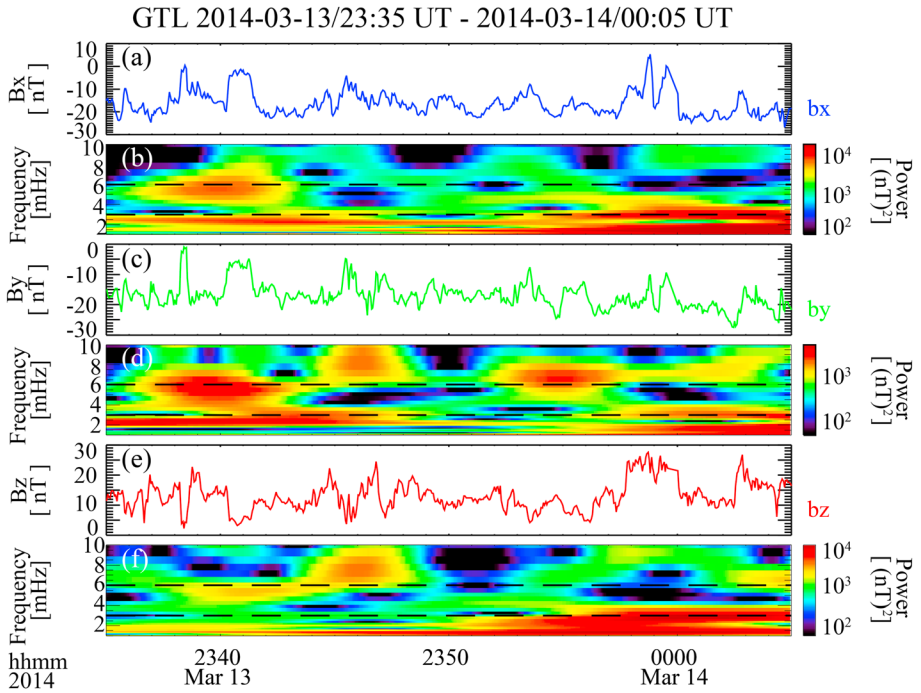

Figure 7. Magnetic data recorded by Geotail and their wavelet spectra for interval 23:35 UT, 13 March, to 00:05 UT, 14 March; the format is the same as in Figure 5. The black dashed line marks the frequency of 3 and 6 mHz, respectively.

frequency, as shown in Figure 6. Therefore, 4 mHz is chosen as the dominant mode frequency of the KHWs recorded by ARTEMIS-P1, and the associated dominant wavelength of the KHWs is about 11.1R_E in the tail.

4. Discussion and Summary

A global MHD simulation (simulation method, see Li et al., 2013) was performed (see Animation S1 in the supporting information) to simulate the magnetospheric response under the average solar wind conditions (V_{sw} = 400 km/s, IMF B_z = 5nT, N = 5 cm^{-3}), which were observed by the WIND spacecraft as shown in Figure 3. Figure 9 shows the simulated X component of the velocity (V_x) in the equatorial plane. The KHWs are formed from the dayside magnetopause to magnetotail, and the continuous development of waves illustrates that the wavelength grows with increasing distance along the magnetopause from the subsolar point. The simulation results support our points obtained from two-point observations, and the increasing KH wavelength has been presented in previous simulations (e.g., Li et al., 2012). If Geotail and ARTEMIS saw the same KHWs, the frequency should be the same or be different by a factor of 2, 4, 8, etc. This is because even if the wavelength or propagation speed are different at the two locations, the oscillations should occur at the same frequency. However, comparison between Figures 6 and 7 shows that this is not the case. It should be noted that in this study, the ARTEMIS and Geotail spacecraft are on different sides of the magnetotail, as shown in Figure 1. It is widely accepted that KHWs can be driven at both flanks (Henry et al., 2017), but a dawn-dusk asymmetry in KHW may occur if ion effects are taken into account. The simulations of Huba (1996), for example, suggested a dawn-dusk asymmetry in the evolution of KHWs in the boundary layer. Hasegawa et al. (2006) reported a nearly symmetric distribution of rolled up KH vortices at both flanks. Taylor et al. (2012) suggested that a dawn-dusk asymmetry in the rolled up KH vortices exists on the dayside but disappears antisunward,

Table 1
The Parameter of Kelvin-Helmholtz Waves Calculated by Geotail and P1 Data

Satellites	Time interval	GSM position (R_E)	T (s)	V (km/s)	λ (R_E)
Geotail	23:35 UT on 13 March to 00:05 UT on 14 March	(−6.6, −8.5, −4.9)	167 and 333	228	5.8 and 11.9
AR-P1	23:35 UT on 13 March to 00:13 UT on 14 March	(−51.0, 32.8, 11.4)	250 and 500	283	11.1 and 22.2

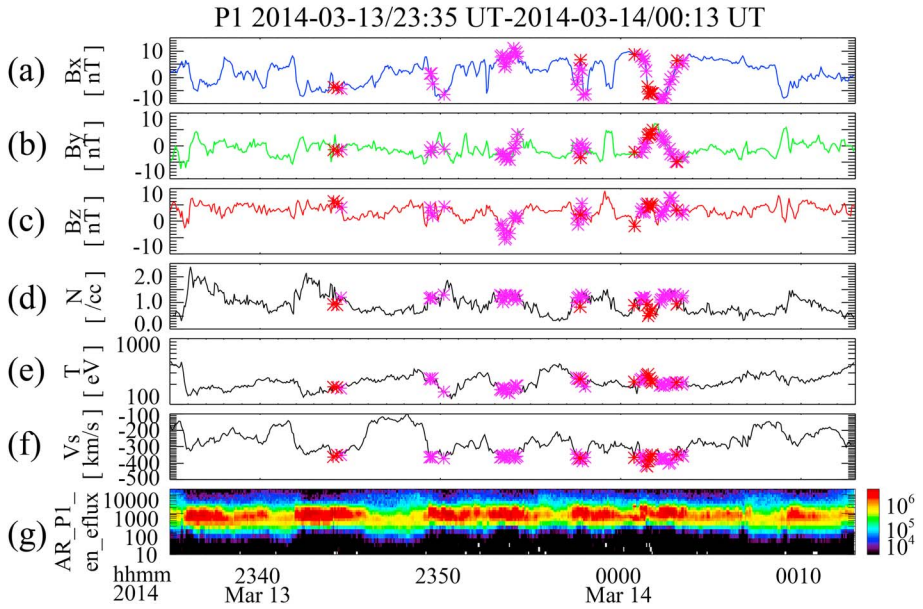

Figure 8. ARTEMIS-P1 data for the time interval 23:35 UT, 13 March, to 00:13 UT, 14 March: (a–c) Three components of the magnetic field, (d) ion number density, (e) average ion temperature, (f) *s* component of the bulk velocity (the *s* direction is antiparallel to the averaged ion velocity for the interval of interest), and (g) energy flux of ions. The red (magenta) points correspond to those in Figure 4a, which are characterized by $V_s < -344$ km/s and $N < 0.9$ cm^{-3} ($N < 1.3$ cm^{-3}).

comparing TC1 events with Geotail events from Hasegawa et al. (2006). Observations from Nishino et al. (2011) showed that KHI vortices grow nearly simultaneously and symmetrically on both flanks, when Geotail and Cluster were located on the opposite sides of the near-Earth magnetotail at almost the same latitude. A dawn-dusk asymmetry was also observed by MESSENGER (e.g., Gershman et al., 2015; Sundberg et al., 2012) in Mercury's magnetosphere and was attributed to spatial scales comparable with an ion gyroradius. Finite Larmor radius effects should affect the instability and lead to asymmetries in the growth rates on the dawn and the dusk flanks (Sundberg et al., 2012). However, the effects of finite Larmor radius are less observable at the Earth since the thickness of the magnetopause current layer is many times the magnetosheath ion Larmor radius (Boardsen et al., 2010). Although the KH wave periods on the Earth's magnetosphere (hundreds of seconds) are many times the periods in MESSENGER KH observations (tens of seconds), Li et al. (2012) proposed that the KH wave periods in Earth's and Mercury's magnetopauses are in a similar band if the different physical dimensions (size, plasma, and magnetic field) of the planetary magnetospheres are taken into account. The simulation results in Figure 9 show rough symmetry of KHWs on the dawn and dusk sides. However, the event shown by Nishino et al. (2011) is for somewhat different solar wind conditions, and the simulation does not include many effects (kinetic, magnetosphere-ionosphere coupling, etc.), whose neglect may not be justifiable for all conditions. We thus cannot completely exclude the presence of dawn-dusk asymmetry in KH vortices in this study. There are two possibilities that may explain the difference in the two-point observations. One is the development of the KHWs as they propagate toward the tail, in consideration of tailward distance between ARTEMIS-P1 and Geotail. The other is the effect of dawn-dusk asymmetry in the KHWs, as the two spacecrafts are on the different sides of the magnetotail.

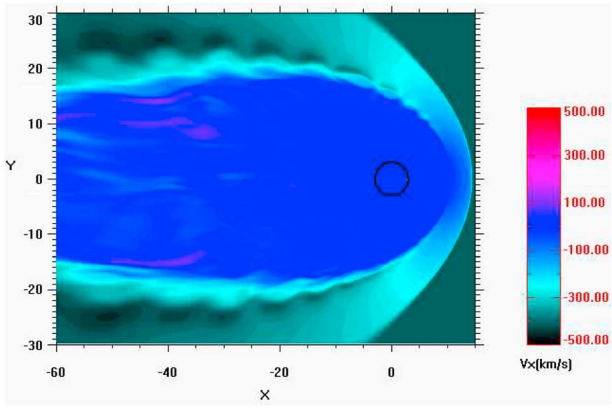

Figure 9. Equatorial cut of the simulated V_x component in GSM coordinates under the average solar wind conditions observed by the WIND spacecraft. It shows that the Kelvin-Helmholtz waves are formed from dayside to nightside magnetopause (see Animation S1 in the supporting information).

In the last section, we show that KHWs with two frequency ranges are observed by both ARTEMIS-P1 and Geotail. This suggests that there may be two spatial scales associated with the KH vortices. Figure 10 shows P1 observations in detail, and at the bottom is shown a

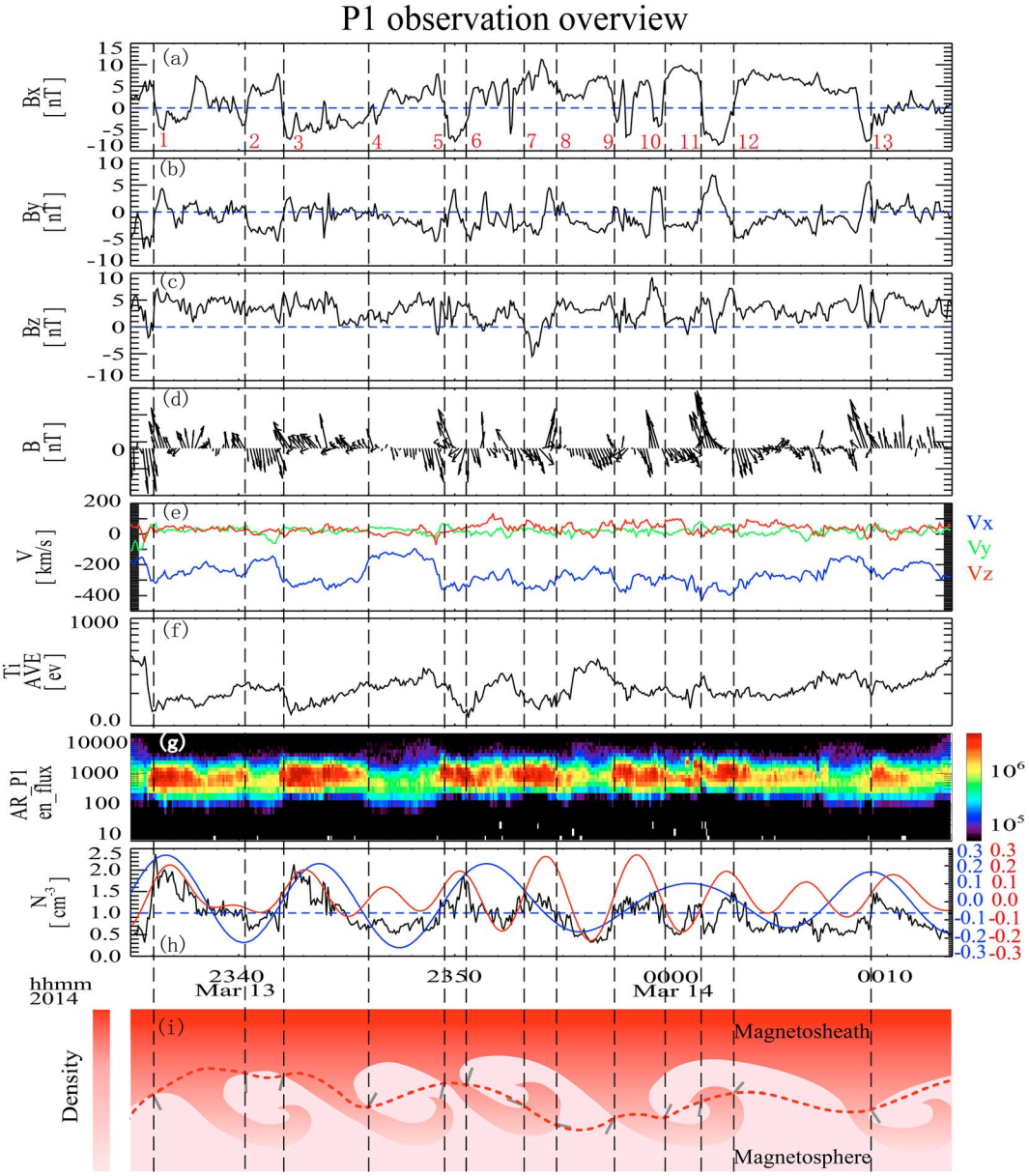

Figure 10. Observations from ARTEMIS-P1 during 23:35 UT, 13 March, to 00:13 UT, 14 March: (a–c) Three components of the magnetic field; (d) the magnitude field fluctuation projected onto GSM_xy plane, (e) ion velocity, V_x (blue), V_y (green), V_z (red); (f) average ion temperature; (g) energy flux of ions; and (h) ion density; the density fluctuation detected by P1 is in black, and the blue and red lines indicate the density data filtered from 1.5 to 2.5 mHz and 3.5 to 4.5 mHz, respectively. (i) Schematic of possible KH vortices encountered by P1 in the equatorial plane. The color code refers to the density, and the dashed line in red shows synthetic spacecraft trajectory. The 13 boundaries between the magnetosheath and the magnetosphere are marked by the vertical black lines and the red numbers, 1–13, in Figure 10a. The short gray lines are boundary normals projected onto the GSM_xy plane.

schematic of rolled-up KH vortices along the magnetopause in the tail. During this interval, P1 encountered the magnetosphere and magnetosheath repeatedly, and the 13 boundaries are characterized by positive (negative) B_x and low (high) density, as marked with vertical black lines and red numbers in Figure 10a. Figure 10i shows a schematic of the KH vortices observed by P1; the upper and lower sides refer to the magnetosphere and magnetosheath, respectively, and a darker color indicates that the density is higher. A minimum variance analysis of the magnetic field (Boardsen et al., 2010) is applied to each boundary crossing to obtain the boundary normal direction, which is then projected onto the GSM *x*-*y* plane. These

normals are shown in Figure 10i by short gray lines. Figure 10h compares the unfiltered density observed by P1 (black curve) with two band-pass filtered density time series (red and blue curves), each with pass-bands of 1 mHz, centered at 2 and 4 mHz, respectively (corresponding to the two frequency ranges obtained from wavelet analysis in Figure 6).

From 23:35 UT to 23:48 UT on 13 March, the unfiltered density variation is consistent with the 2-mHz filtered data, and a 4-mHz component appears to become more significant for times after 23:50 UT on 13 March. This suggests that P1 may have passed a larger spatial structure at first, and then the satellite moved closer to the center of the vortex and encountered substructures. We provide two possible explanations for the formation mechanism of substructures within the larger vortex. First, the feature could be associated with the time evolution of the KHWs, as they develop along the magnetopause and evolve into the nonlinear stage where rolled-up vortices appear. At this stage of the KHW evolution process, the wavelength would increase; however, the waveform becomes multivalued. In other words, the smaller scale is observed because of strongly rolled-up vortices due to the nonlinear evolution of KHWs. The second possibility is that smaller structures associated with higher-frequency vortices become coupled and then form a larger one as the KHWs propagate tailward, supporting the so-called "inverse cascade" mechanism (Belmont & Chanteur, 1989).

In this paper, we present simultaneous observations of KHWs by the ARTEMIS spacecraft (P1 and P2) and Geotail at different locations when the IMF is dominantly northward and provide observational evidence for solar wind-magnetosphere interactions in the tail region near the lunar orbit. The KHWs are studied by using quantitative methods to calculate the dominant period, phase velocity, and wavelength. By a comparison of the results between these two satellites, we can infer that either (i) the phase velocity and the spatial scale of the KHWs tend to increase along the boundary layer when the waves propagate tailward or (ii) the difference between dawnside and duskside observations is due to the influence of dawn-dusk asymmetry. The KHWs with two frequency ranges are observed by these satellites, indicating multiscale development of KHWs in the nonlinear stage. The time evolution of KHWs and processes within rolled-up vortices that facilitate plasma transport and mixing still remain unclear. Therefore, more observational studies to clarify these unsolved questions will be required.

Acknowledgments

We acknowledge NASA contract NAS5-02099 and V. Angelopoulos for use of data from the THEMIS Mission (http://themis.ssl.berkeley.edu /data/themis/). We also acknowledge the use of Geotail data obtained from Data ARchives and Transmission System (DARTS), provided by the Center for Science-satellite Operation and Data Archive (C-SODA) at ISAS/JAXA (http://www.darts.isas.jaxa.jp/stp/geotail/). The IMF information from the WIND satellite was through the CDA web (http://cdaweb.gsfc.nasa.gov/). This work was supported by the National Natural Science Foundation of China (grants 41574157, 41628402, 41322031, and 41774153), and the SNSB grant 77/14. A. N. F. is funded in part by STFC grant ST/N0007722/1, and I. J. R. is funded in part by STFC grant ST/N0007722/1 and NERC grants NE/L007495/1, NE/P017150/1, and NE/P017185/1. The project was also supported by the specialized research fund for State Key Laboratories.

References

Angelopoulos, V. (2008). The THEMIS mission. *Space Science Reviews*, *141*(1-4), 5–34. https://doi.org/10.1007/s11214-008-9336-1

Auster, H. U., Glassmeier, K. H., Magnes, W., Aydogar, O., Baumjohann, W., Constantinescu, D., et al. (2008). The THEMIS fluxgate magnetometer. *Space Science Reviews*, *141*(1-4), 235–264. https://doi.org/10.1007/s11214-008-9365-9

Belmont, G., & Chanteur, G. (1989). Advances in magnetopause Kelvin-Helmholtz instability studies. *Physica Scripta*, *40*(1), 124–128. https://doi.org/10.1088/0031-8949/40/1/018

Boardsen, S. A., Sundberg, T., Slavin, J. A., Anderson, B. J., Korth, H., Solomon, S. C., & Blomberg, L. G. (2010). Observations of Kelvin-Helmholtz waves along the dusk-side boundary of Mercury's magnetosphere during MESSENGER's third flyby. *Geophysical Research Letters*, *37*, L12101. https://doi.org/10.1029/2010GL043606

Chandrasekhar, S. (1961). *Hydrodynamic and hydromagnetic stability*. New York: Oxford University Press.

Chen, L., & Hasegawa, A. (1974). A theory of long-period magnetic pulsations: 1. Steady state excitation of field line resonance. *Journal of Geophysical Research*, *79*, 1033–1037. https://doi.org/10.1029/JA079i007p01033

Dungey, J. W. (1962). The interplanetary magnetic field and the auroral zones. *Physical Review Letters*, *6*(2), 47–48. https://doi.org/10.1103/PhysRevLett.6.47

Eriksson, S., Lavraud, B., Wilder, F. D., Stawarz, J. E., Giles, B. L., Burch, J. L., et al. (2016). Magnetospheric Multiscale observations of magnetic reconnection associated with Kelvin-Helmholtz waves. *Geophysical Research Letters*, *43*, 5606–5615. https://doi.org/10.1002/2016GL068783

Eriksson, S., Wilder, F. D., Ergun, R. E., Schwartz, S. J., Cassak, P. A., Burch, J. L., et al. (2016). Magnetospheric Multiscale observations of the electron diffusion region of large guide field magnetic reconnection. *Physical Review Letters*, *117*(1), 015001. https://doi.org/10.1103/PhysRevLett.117.015001

Fairfield, D. H., Otto, A., Mukai, T., Kokubun, S., Lepping, R. P., Steinberg, J. T., et al. (2000). Geotail observations of the Kelvin-Helmholtz instability at the equatorial magnetotail boundary for parallel northward fields. *Journal of Geophysical Research*, *105*, 21,159–21,173. https://doi.org/10.1029/1999JA000316

Foullon, C., Farrugia, C. J., Fazakerley, A. N., Owen, C. J., Gratton, F. T., & Torbert, R. B. (2008). Evolution of Kelvin-Helmholtz activity on the dusk flank magnetopause. *Journal of Geophysical Research*, *113*, A11203. https://doi.org/10.1029/2008JA013175

Gershman, D. J., Raines, J. M., Slavin, J. A., Zurbuchen, T. H., Sundberg, T., Boardsen, S. A., et al. (2015). MESSENGER observations of multiscale Kelvin-Helmholtz vortices at Mercury. *Journal of Geophysical Research*, *120*, 4354–4368. https://doi.org/10.1002/2014JA020903

Gou, X. C., Shi, Q. Q., Tian, A. M., Sun, W. J., Dunlop, M. W., Fu, S. Y., et al. (2016). Solar wind plasma entry observed by cluster in the high-latitude magnetospheric lobes. *Journal of Geophysical Research*, *121*, 4135–4144. https://doi.org/10.1002/2015JA021578

Hasegawa, H. (2012). Structure and dynamics of the magnetopause and its boundary layers. *Monographs on Environment, Earth and Planets*, *1*(2), 71–119. https://doi.org/10.5047/meep.2012.00102.0071

Hasegawa, H., Fujimoto, M., Phan, T. D., Rème, H., Balogh, A., Dunlop, M. W., et al. (2004). Transport of solar wind into Earth's magnetosphere through rolled-up Kelvin-Helmholtz vortices. *Nature*, *430*(7001), 755–758. https://doi.org/10.1038/nature02799

Hasegawa, H., Fujimoto, M., Takagi, K., Saito, Y., Mukai, T., & Re'me, H. (2006). Single-spacecraft detection of rolled-up Kelvin-Helmholtz vortices at the flank magnetopause. *Journal of Geophysical Research*, *111*, A09203. https://doi.org/10.1029/2006JA011728

Hasegawa, H., Retino, A., Vaivads, A., Khotyaintsev, Y., An-dre, M., Nakamura, T. K. M., et al. (2009). Kelvin-Helmholtz waves at the earth's magnetopause: Multiscale development and associated reconnection. *Journal of Geophysical Research*, *114*, A12207. https://doi.org/10.1029/2009JA014042

Henry, Z. W., Nykyri, K., Moore, T. W., Dimmock, A. P., & Ma, X. (2017). On the dawn-dusk asymmetry of the Kelvin-Helmholtz instability between 2007 and 2013. *Journal of Geophysical Research*, *122*, 11,888–11,900. https://doi.org/10.1002/2017JA024548

Huba, J. D. (1996). The Kelvin-Helmholtz instability: Finite Larmor radius magnetohydrodynamics. *Geophysical Research Letters*, *23*, 2907–2910. https://doi.org/10.1029/96GL02767

Kavosi, S., & Raeder, J. (2015). Ubiquity of Kelvin–Helmholtz waves at Earth's magnetopause. *Nature Communications*, *6*(1), 7019. https://doi.org/10.1038/ncomms8019

Kokubun, S., Yamamoto, T., Acuna, M. H., Hayashi, K., Shiokawa, K., & Kawano, H. (1994). The Geotail magnetic field investigation. *Journal of Geomagnetism and Geoelectricity*, *46*, 7.

Li, W., André, M., Khotyaintsev, Y. V., Vaivads, A., Graham, D. B., Toledo-Redondo, S., et al. (2016). Kinetic evidence of magnetic reconnection due to Kelvin-Helmholtz waves. *Geophysical Research Letters*, *43*, 5635–5643. https://doi.org/10.1002/2016GL069192

Li, W. Y., Guo, X. C., & Wang, C. (2012). Spatial distribution of Kelvin-Helmholtz instability at low-latitude boundary layer under different solar wind speed conditions. *Journal of Geophysical Research*, *117*, A08230. https://doi.org/10.1029/2012JA017780

Li, W. Y., Wang, C., Tang, B., Guo, X., & Lin, D. (2013). Global features of Kelvin-Helmholtz waves at the magnetopause for northward interplanetary magnetic field. *Journal of Geophysical Research*, *118*, 5118–5126. https://doi.org/10.1002/jgra.50498

Lin, D., Wang, C., Li, W., Tang, B., Guo, X., & Peng, Z. (2014). Properties of Kelvin-Helmholtz waves at the magnetopause under northward interplanetary magnetic field: Statistical study. *Journal of Geophysical Research*, *119*, 7485–7494. https://doi.org/10.1002/2014JA020379

Liu, Y., Lei, J., Yu, P., Liu, P., Ling, Y., Zhang, Z., & Cao, J. (2018). Spontaneous emission of Alfvénic branch oscillations from a strong inhomogeneous plasma flow. *Geophysical Research Letters*, *45*, 64–70. https://doi.org/10.1002/2017GL075611

Matsumoto, Y., & Hoshino, M. (2004). Onset of turbulence induced by a Kelvin-Helmholtz vortex. *Geophysical Research Letters*, *31*, L02807. https://doi.org/10.1029/2003GL018195

McFadden, J. P., Carlson, C. W., Larson, D., Ludlam, M., Abiad, R., Elliott, B., et al. (2008). The THEMIS ESA plasma instrument and in-flight calibration. *Space Science Reviews*, *141*(1-4), 277–302. https://doi.org/10.1007/s11214-008-9440-2

Mitchell, D. G., Kutchko, F., Williams, D. J., Eastman, T. E., Frank, L. A., & Russell, C. T. (1987). An extended study of the low-latitude boundary layer on the dawn and dusk flanks of the magnetosphere. *Journal of Geophysical Research*, *92*, 7394–7404. https://doi.org/10.1029/JA092iA07p07394

Miura, A. (1999). A quantitative test of the self-organization hypothesis of the magnetopause Kelvin-Helmholtz instability as an inverse problem. *Geophysical Research Letters*, *26*, 409–412. https://doi.org/10.1029/1998GL900300

Mukai, T., Machida, S., Saito, Y., Hirahara, M., Terasawa, T., Kaya, N., et al. (1994). The low energy particle (LEP) experiment on board the Geotail satellite. *Journal of Geomagnetism and Geoelectricity*, *46*(8), 669–692. https://doi.org/10.5636/jgg.46.669

Nakamura, T. K. M., Hayashi, D., Fujimoto, M., & Shinohara, I. (2004). Decay of MHD-scale Kelvin-Helmholtz vortices mediated by parasitic electron dynamics. *Physical Review Letters*, *92*(14), 145001. https://doi.org/10.1103/PhysRevLett. 92.145001

Nishino, M. N., Hasegawa, H., Fujimoto, M., Saito, Y., Mukai, T., Dandouras, I., et al. (2011). A case study of Kelvin-Helmholtz vortices on both flanks of the Earth's magnetotail. *Planetary and Space Science*, *59*, 502–509. https://doi.org/10.1016/j.pss.2010.03.011

Rae, I. J., Donovan, E. F., Mann, I. R., Fenrich, F. R., Watt, C. E. J., Milling, D. K., et al. (2005). Evolution and characteristics of global Pc5 ULF waves during a high solar wind speed interval. *Journal of Geophysical Research*, *110*, A12211. https://doi.org/10.1029/2005JA011007

Shi, Q. Q., Zong, Q.-G., Fu, S. Y., Dunlop, M. W., Pu, Z. Y., Parks, G. K., et al. (2013). Solar wind entry into the high-latitude terrestrial magnetosphere during geomagnetically quiet times. *Nature Communications*, *4*, 1466. https://doi.org/10.1038/ncomms2476

Shue, J.-H., Song, P., Russell, C. T., Steinberg, J. T., Chao, J. K., Zastenker, G., et al. (1998). Magnetopause location under extreme solar wind conditions. *Journal of Geophysical Research*, *103*(A8), 17,691–17,700. https://doi.org/10.1029/98JA01103

Song, P., & Russell, C. T. (1992). Model of the formation of the low-latitude boundary-layer for strongly northward interplanetary magnetic-field. *Journal of Geophysical Research*, *97*, 1411–1420. https://doi.org/10.1029/91JA02377

Sonnerup, B. U. O., & Scheible, M. (1998). Minimum and maximum variance analysis. In G. Paschmann & P. W. Daly (Eds.), *Analysis methods for multi-spacecraft data* (pp. 185–220). Bern: European Space Agency.

Sundberg, T., Boardsen, S. A., Slavin, J. A., Anderson, B. J., Korth, H., Zurbuchen, T. H., et al. (2012). MESSENGER orbital observations of large-amplitude Kelvin-Helmholtz waves at Mercury's magnetopause. *Journal of Geophysical Research*, *117*, A04216. https://doi.org/10.1029/2011JA017268

Takagi, K., Hashimoto, C., Hasegawa, H., Fujimoto, M., & TanDokoro, R. (2006). Kelvin-Helmholtz instability in a magnetotail flank-like geometry: Three-dimensional MHD simulations. *Journal of Geophysical Research*, *111*, A08202. https://doi.org/10.1029/2006JA011631

Taylor, M. G. G. T., Hasegawa, H., Lavraud, B., Phan, T., Escoubet, C. P., Dunlop, M. W., et al. (2012). Spatial distribution of rolled up Kelvin-Helmholtz vortices at Earth's dayside and flank magnetopause. *Annales Geophysicae*, *30*(6), 1025–1035. https://doi.org/10.5194/angeo-30-1025-2012

Taylor, M. G. G. T., Lavraud, B., Escoubet, C. P., Milan, S. E., Nykyri, K., Dunlop, M. W., et al. (2008). The plasma sheet and boundary layers under northward IMF: A multipoint and multi-instrument perspective. *Advances in Space Research*, *41*(10), 1619–1629. https://doi.org/10.1016/j.asr.2007.10.013

Terasawa, T., Fujimoto, M., Mukai, T., Shinohara, I., Saito, Y., Yamamoto, T., et al. (1997). Solar wind control of density and temperature in the near-earth plasma sheet: Wind/geotail collaboration. *Geophysical Research Letters*, *24*, 935–938. https://doi.org/10.1029/96GL04018

Wang, C.-P., Merkin, V. G., & Angelopoulos, V. (2017). Mesoscale perturbations in midtail lobe/mantle during steady northward IMF: ARTEMIS observation and MHD simulation. *Journal of Geophysical Research: Space Physics*, *122*, 6430–6441. https://doi.org/10.1002/2017JA024305

Wang, C.-P., Thorne, R., Liu, T. Z., Hartinger, M. D., Nagai, T., Angelopoulos, V., et al. (2017). A multispacecraft event study of Pc5 ultralow-frequency waves in the magnetosphere and their external drivers. *Journal of Geophysical Research: Space Physics*, *122*, 5132–5147. https://doi.org/10.1002/2016JA023610